Conditional Color Gamut for Color Management of Multiview Printed Images

Nicolas Dalloz[1,2(✉)] and Mathieu Hébert[1]

[1] Univ Lyon, UJM-Saint-Etienne, CNRS, Institut d Optique Graduate School, Laboratoire Hubert Curien, UMR 5516, Saint-Etienne, France
[2] HID Global CID SAS, Suresnes, France
nicolas.dalloz@hidglobal.com

Abstract. A number of printing or surface coloration technologies have recently emerged, able to print color images on various kinds of supports with various benefits in terms of color rendering. Some of them are even able to produce image with variable colors, where each point in the print can display two or more colors according to the illumination or observation conditions (modes). For most printing systems presenting these variable color properties, the colors displayable in one mode depend on the colors that we want to display in the other modes. Because of this interdependence of the colors displayable in the different modes, the color gamut concept as defined for traditional printing is not sufficient anymore to perform efficient color management. We propose to extend it by taking into account the constraints induced by the selection of colors in some modes, and introduce the concept of conditional color gamut, illustrated through the case of recto-verso halftone prints viewed in reflection or transmission modes, where gamuts can be easily predicted thanks to prediction models.

Keywords: Color reproduction · Computational printing · Recto-verso printing · Multiview printed image

1 Introduction

The color reproduction domain, associated with computational printing, evolves rapidly towards new usages and observation scenarios for which the color management methods developed for standard 2D printing are not directly adapted. Methods relying on ICC profiles often fail with these new printing technologies, mainly because of the number of measurements which would be required. This is especially true in the case of multi-ink printing, more and more used for a spectral reproduction instead of simply color reproduction [1–4], or in the case of 2.5 and 3D printings which intend to reproduce not only color but also other visual attributes such as gloss, texture and translucency [5–7]. This is also true in the case of the multi-view printing technologies which emerge thanks to the progress of computational printing [8–11] or plasmonic color effects [12–16]. Multi-view prints are surfaces (or multilayer supports) able to display different colors, and even different images, according to the way they are illuminated and/or observed. Their characterization is not necessarily a big challenge, except in the case of the plasmonic surfaces which are often very specular and need a

S. Tominaga et al. (Eds.): CCIW 2019, LNCS 11418, pp. 63–76, 2019.
https://doi.org/10.1007/978-3-030-13940-7_6

high measurement precision offered only by specific optical instrumentation [17], and probably also extended perception models for their structural colors. But for the technologies based on more conventional printing, for example paper with special inks [8–10], standard inks on special supports [11], or recto-verso prints viewed in reflection or transmission [18, 19], usual spectrophotometers often suffice. The main difficulty lies on the fact that the colors achievable in one viewing mode may depend on the color targeted in the other modes [20]. This is obvious with structural colors, where the micro- or nano-structure determines the colors displayed under every angle and polarization of the incident light. In ink-based printing, the presence of a certain amount of inks on the support gives a certain tint to the print in all viewing modes, or at least discards certain colors in some modes. The color management methods which seem to have been used so far to obtain the multi-view color images in the contributions mentioned above rely either on manual color selections, or on look-up tables listing expansively the sets of displayable colors in the different viewing modes according to the printing command parameters, i.e. on time-consuming methods which need to be repeated each time one parameter is modified in the printing setup.

In order to cope with the issue of interdependence of the colors displayable in different viewing modes, we propose to refine the color gamut concept while including these interdependence constraints, by introducing the concept of conditional color gamut. This concept could be illustrated through any multi-view printing technology. We selected the recto-verso halftone printing on paper for observation in reflection and transmission, whose color gamuts can be easily generated thanks to the accurate spectral reflectance and transmittance models available today, and whose advantage is also to be familiar to anybody as it is close to conventional ink printing.

The paper is structured as follows: first, in Sect. 2, we present the characteristics of recto-verso halftone prints and review the models allowing the prediction of their spectral reflectance and transmittance, thereby their color in reflection and transmission modes. We show the color gamuts associated with these modes for office paper printed on both sides with an electrophotography printer. In Sect. 3, we introduce the concept of conditional color gamut after having explained the constraints on the reproduction of certain colors in the transmission mode once the colors in the reflection mode have been selected. The interest of the conditional color gamut concept is revealed in Sect. 4 when we want to display different images in reflection and transmission modes, which requires to match the colors of different areas of the print based on different recto-verso halftones. We show that the intersection of conditional color gamuts is a convenient way to verify that color matching is possible, or to select colors in the two modes such that we are certain that color matching is possible. In Sect. 5, we address the question of the contrast which can be obtained in the images displayed in the reflectance and transmittance modes, knowing that in recto-verso printing, a good contrast in one of the two mode is to the detriment of the contrast in the other mode [20]. Section 6 finally draws the conclusions.

2 Recto-Verso Print in Different Illumination Conditions

A recto-verso color print is a support, preferably strongly scattering but not opaque, printed on both sides with different halftone colors, each halftone being characterized by the surface coverages of the different inks. As the examples presented hereinafter

will be based on CMY color printing, we will denote as c, m, y the surface coverage of the three inks cyan, magenta and yellow on the recto side, and c', m', y' their surface coverage on the verso side. Four flux transfer factors characterize the macroscopic optical properties of the print: its reflectance $R(\lambda)$ and transmittance $T(\lambda)$ for an illumination of the recto side, and its reflectance $R'(\lambda)$ and transmittance $T'(\lambda)$ for an illumination of the verso side (Fig. 1).

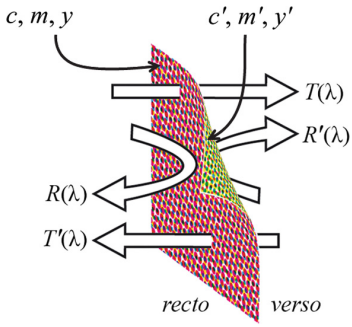

Fig. 1. Flux transfers in a recto-verso print. (Color figure online)

We usually consider that the observer looks at the recto side of the print, whose color appearance vary according to the illumination of the two sides. In the most general case, the irradiances on the recto and verso sides can be different, with different spectral power distributions (SPDs) and different magnitudes. We will consider in this study that the two irradiances have similar SPDs, denoted as $E_i(\lambda)$, and only their magnitude can differ. In the case where only the recto side is lit, we are in the *reflectance mode*. The observer received the spectral radiance:

$$L_R(\lambda) = \frac{1}{\pi} R(\lambda) E_i(\lambda) \tag{1}$$

In the opposite case where the print is backlit without illumination of the recto side, we are in the *transmittance mode*, and the observed radiance is:

$$L_T(\lambda) = \frac{1}{\pi} T'(\lambda) E_i(\lambda) \tag{2}$$

In the case where light comes from both sides, with an irradiance $(1 - \alpha)E_i(\lambda)$ on the recto side and an irradiance $\alpha E_i(\lambda)$ on the verso side, we are in an α-*transmittance mode*, and the observed radiance is:

$$L_{\alpha T}(\lambda) = \frac{1}{\pi} [(1 - \alpha) R(\lambda) E_i(\lambda) + \alpha T'(\lambda) E_i(\lambda)] \tag{3}$$

The pure reflectance and transmittance modes correspond respectively to $\alpha = 0$, and $\alpha = 1$. The reflectance mode is usual: each time we read a document, a newspaper or a book, we are in this configuration since we generally avoid backlighting. The pure transmittance mode is rarer because it needs to prevent ambient light susceptible to illuminate the recto side, therefore to be in the dark. The α-T transmittance mode corresponds to the lighting configuration where we have ambient light and a light source (e.g. a window) behind the document that we are reading. We estimated that when a document is viewed in front of the window of a white room, α is around 0.9 [20].

Various models are now available to predict the spectral reflectance and transmittance of recto-verso prints, therefore their color in the different illumination scenarios mentioned above. The first model proposed by Hébert and Hersch [21, 22] extends the Clapper-Yule [23] and Williams-Clapper models [24] thanks to a generalized two-flux approach. The reflectance model is calibrated from reflectance measurements on a limited number of halftone patches printed on the recto side, permitting to assess the intrinsic optical parameters of the support and the inks as well as the ink dot spreading on the support [25]. The transmittance model is calibrated from transmittance measurement on the same set of halftone color patches as the one used for calibrating the reflectance model. Recent improvements of this two-flux approach have been proposed by Mazauric *et al.* by using flux transfer matrices, leading to the Duplex printing reflectance-transmittance (DPRT) model [19], and the Double-layer reflectance transmittance (DLRT) model [18]. Another family of models extend the Yule-Nielsen modified spectral Neugebauer model which has become classical for the reflectance prediction of halftone prints: a first version for the transmittance of recto-verso prints has been proposed by Hebert and Hersch [26], again refined by Mazauric *et al.* by using flux transfer matrices and avoiding the empirical determination of the Yule-Nielsen n parameter [27]. These different approaches provide good prediction accuracy for conventional printing on common or high quality papers, or white polymer supports.

Throughout the present paper, we will consider a printing setup based on a common 80 g/m^2 office paper, printed on both sides with the Xerox Phaser 6500DN PS electrophotography printer, by using only the cyan, magenta and yellow inks (no black ink) deposited according to a rotated clustered dot halftoning technique at 120 lpi. The paper is similar on both sides, and the same printer, inks and halftoning technique are used on both sides. The DLRT model [18], specially calibrated for this printing setup, has shown good prediction accuracy, with an average ΔE94 value of 0.89 unit between predicted and measured spectra over a large set recto-verso halftone colors used for verification of the model. The good color prediction accuracy is also confirmed by the color matching between different recto-verso halftone colors that we could obtain on real prints with ink surface coverages computed by using the DLRT model in an inversed approach, as shown later in Figs. 4 and 6.

We thus predicted thanks to the DLRT model the spectral reflectances and transmittances of 11^6 recto-verso halftone colors where each of the surface coverages c, m, y, c', m', y' varies from 0 to 1 in steps of 0.1. The predicted spectral reflectances and transmittances were converted into spectral radiances perceived in reflection mode, resp. transmission mode, according to Eq. (1), resp. Eq. (2), by considering an irradiance $E_i(\lambda)$ whose SPD corresponds to the one of the D65 illuminant. The spectral radiances were then converted into CIE1931 XYZ tristimulus values, then into

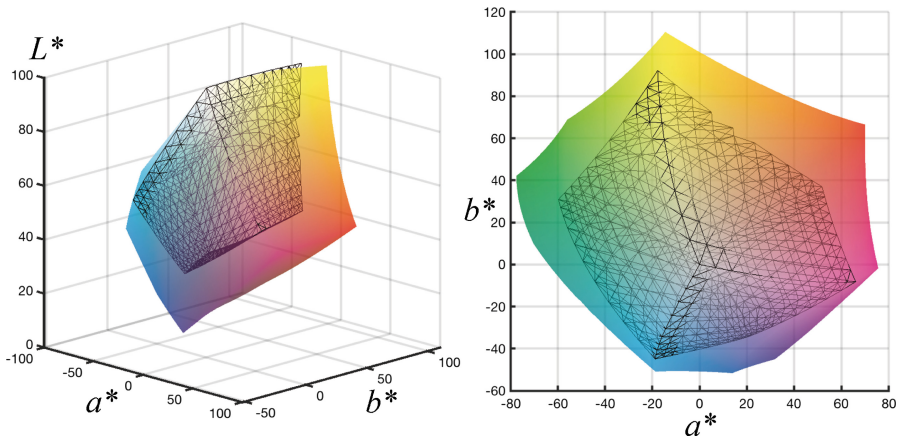

Fig. 2 Color gamuts obtained in reflection mode (volumes featured by the black meshed surface) and transmission mode (featured by the volumes in color) for common office paper printed on both sides with an electrophotography printer. (Color figure online)

CIE1976 L*a*b* color coordinates by using the XYZ tristimulus values of the unprinted paper as "white stimulus" for the chromatic adaptation [28].

The obtained color gamuts in reflection and transmission modes are shown in Fig. 2. In reflection mode, the colors are due only to the inks printed on the recto side, whereas in transmission mode, they are determined by the inks printed on both sides. The gamut in transmission mode looks larger than the one in reflection mode. This is a consequence of the white color selected for the conversion of the XYZ tristimulus values into L*a*b* color coordinates, corresponding to the tristimulus values of the unprinted paper in each mode. Notice that the radiance of the unprinted white depends on the observation mode, as it can be seen in Fig. 4, but it has the highest luminance in each mode. It is therefore suitable to use it as the "white stimulus" in the calculation of the CIE1976 L*a*b* color coordinates, in observation scenarios where nothing around the print is brighter than the unpinted paper. This is not obvious in the transmission mode where the light source behind the print can be observed simultaneously with the print. We assume here that the light source is not visible, but this has no consequence on the concepts developed in the next sections.

Notice that an α-transmission mode, with $0 < \alpha < 1$, would yield a gamut different from the ones displayed in Fig. 2.

The color gamut concept is central in color reproduction to ensure optimal reliability of the printed colors in comparison to the original image that we want to print. For example, gamut mapping techniques, known to provide optimal color rendering for images reproduced with a given printing system, rely on this color gamut concept [29]. However, gamut mapping is possible only in one illumination-observation mode, based on the gamut associated with this mode. When the print is intended to be observed in more than one mode, we must take into account the fact that the color wanted in one mode can constrain the colors reproducible in the other modes. As far as we know, no

"multi-gamut mapping" technique has ever been proposed which could take these constraints into consideration. One first step towards this direction relies on the concept of conditional color gamut that we introduce in the next section.

3 Conditional Color Gamut

When the print is intended to be viewed in more than one illumination mode, in our case in the reflection and transmission modes, the set of colors reproducible in one mode may depend upon the colors that we want to display in the other modes. For example, if we want a yellow color in reflection mode, we must print on the recto side of the support a halftone color containing mainly yellow ink; consequently, whatever is the halftone color printed on the verso side, the color viewed in transmission mode will necessarily look yellowish. The set of colors actually displayable in the transmission mode is reduced in comparison to the global color gamut in this mode, and we will call this reduced set "conditional color gamut in transmission mode associated with this yellow color wanted in reflection mode".

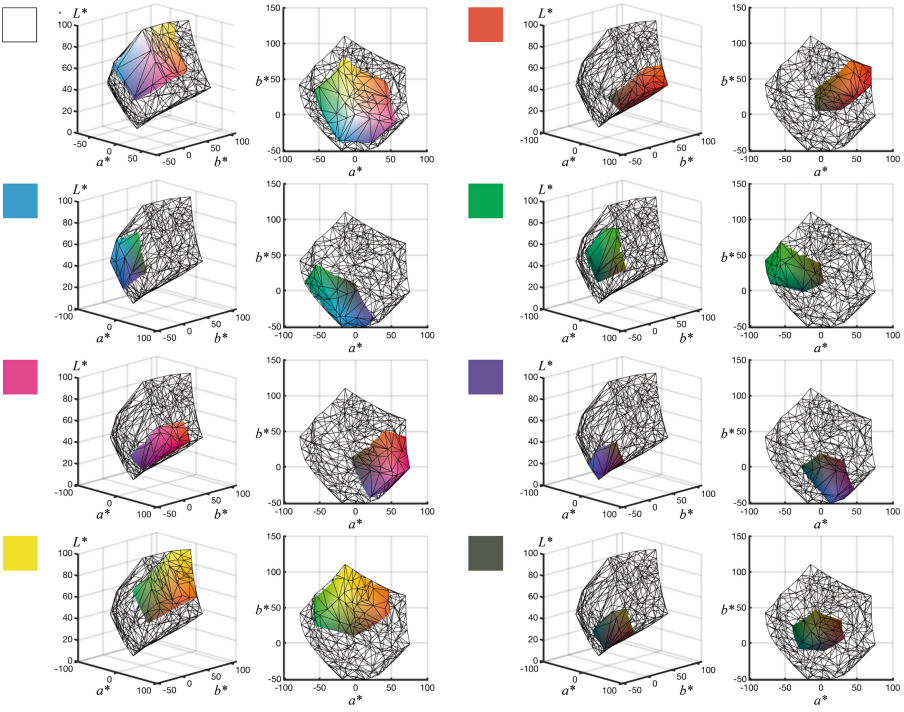

Fig. 3 Conditional color gamuts $G_t(C_r)$ in transmittance mode shown under two different points view in the CLE1976 L*a*b* color space, associated with eight different colors C_r wanted in reflectance mode featured by the colored squares on the left of the gamuts. The volumes featured by a meshed surface correspond to the global color gamut in transmittance mode, already displayed in color in Fig. 2. (Color figure online)

More generally, we will denote as $G_t(C_r)$ the conditional color gamut in transmission mode associated with a color C_r in reflection mode. Figure 3 shows eight examples of conditional color gamuts associated with eight different colors selected for the reflection mode corresponding to the eight Neugebauer primaries that we have in CMY printing: white ($c = m = y = 0$), cyan ($c = 1$, $m = y = 0$), magenta ($c = y = 0$, $m = 1$), yellow ($c = m = 0$, $y = 1$), red ($c = 0$, $m = y = 1$), green ($c = y = 1$, $m = 0$), blue ($c = m = 1$, $y = 0$), and black ($c = m = y = 1$). For each color C_r, we considered the 11^3 halftone colors on the verso side where c', m', y' are varied from 0 to 1 in steps of 0.1, we predicted the spectral transmittances of these recto-verso halftone patches, and converted them into CIE1976 L*a*b* color coordinates. The obtained conditional gamut is displayed under the form of a color volume and compared to the global gamut associated with the transmission mode, already shown as a color volume in Fig. 2 and represented here by the black meshed surfaces.

If we focus on the case of the yellow color in the reflection mode, displayed at the bottom left of the figure, we clearly see that the corresponding conditional color gamut is a small subset of the global conditional gamut associated with the transmission mode, and covers only the most yellowish colors.

4 Color Matching and Intersection of Conditional Color Gamuts

The interest of prints displaying different colors in different illumination modes is the possibility to display with one printed support different images or graphical contents in the different modes. Figure 4 shows a simple example of paper printed with the same printing setup as the one described in Sect. 4, displaying two different images in reflection and transmission modes, one containing four colors, the other one containing two gray colors. The printed area is a square subdivided into four squares with same area, surrounded by the unprinted paper whose color, different in the two modes, is considered as the white reference for the calculation of the CIE1976 L*a*b* color coordinates in each mode. In the reflection mode, the four squares have four different colors, labelled C_{r1}, C_{r2}, Cr_3 and C_{r4}. In transmission mode, the two squares on the top

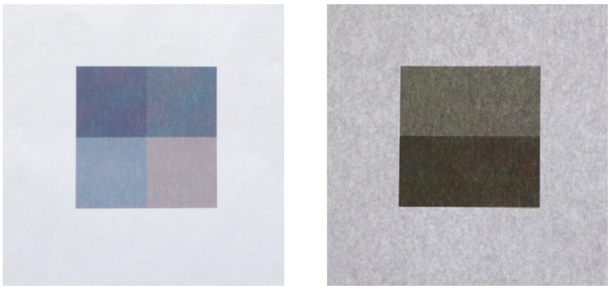

Fig. 4 Recto-verso print produced with the printing setup described in Sect. 4, viewed in (a) reflectance mode, and (b) transmittance mode (uncalibrated color pictures). (Color figure online)

have the same gray color C_{t1} and the two square on the bottom have the same gray color C_{r2}, thus forming the image composed of two gray rectangles. Notice that the color pictures have been taken with an uncalibrated camera.

The possibility to display four colors in reflection mode and only two colors in transmission mode relies on a color matching operation: the four halftone colors printed on the recto side have been selected in order to obtain identical colors in transmission mode for the two squares on the top, and for the two squares on the bottom. The frontier between the squares is not visible anymore inside the rectangles.

Obtaining one color C_{t1} in transmission mode knowing that two colors C_{r1} and C_{r2} are displayed in reflection mode means that C_{t1} belong to both conditional gamuts $G_t(C_{r1})$ and $G_t(C_{r2})$, therefore to the intersection of the two conditional gamuts, $G_t(C_{r1}) \bigcap G_t(C_{r2})$. The color matching between the two areas is possible when the intersection is non-empty, and any other color belonging to the intersection could have been selected to fulfill the rectangle.

Figure 5 shows a pair of conditional color gamuts in transmittance mode (featured by the black meshed surfaces) associated with a pair of gray colors wanted in reflection mode, as well as their intersection represented by the volume in red whose size is assessed by a volume quantity V expressed in arbitrary unit. This volume of intersection is computed as follows [30]: since each conditional gamut is originally represented by a set of points in the CIE1976 L*a*b* color space computed from a set of predicted spectral transmittances, an alpha-shape is computed from this set of points in order to draw its envelope, thanks to the function *alphaShape* in Matlab©. The alpha value was set to 30, which gives a satisfying accuracy of the 3D shape. Once the

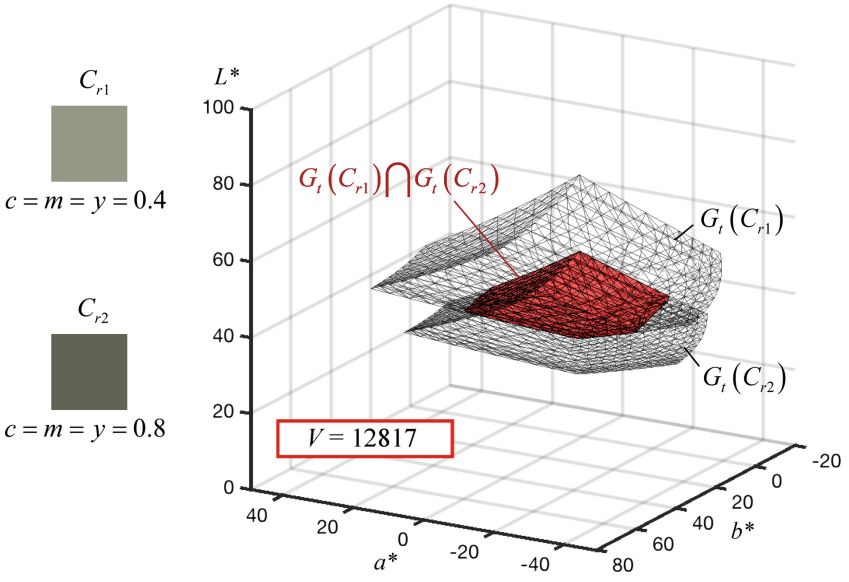

Fig. 5 Conditional color gamuts $G_t(C_{r1})$ and $G_t(C_{r2})$ in transmission mode associated with four different pairs of gray colors C_{r1} and C_{r2} wanted in the reflection mode (meshed surfaces), and their intersection (volume in red). (Color figure online)

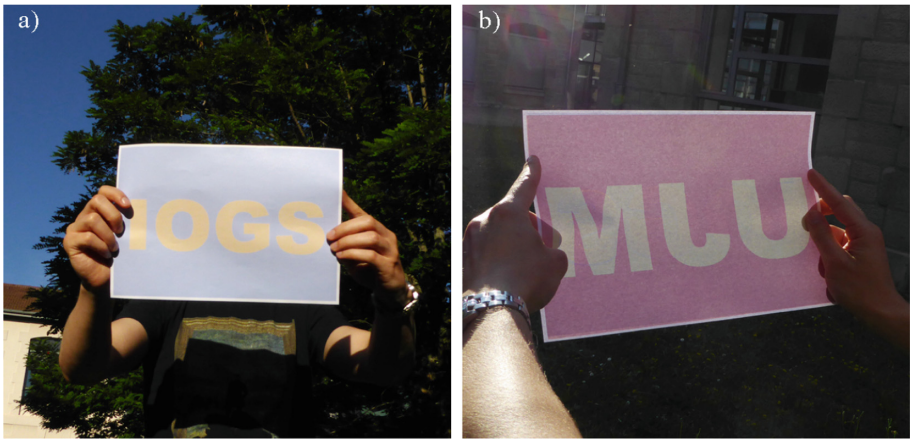

Fig. 6 Recto-verso print printed in inkjet showing two different binary color images in (a) reflectance mode, and (b) transmittance mode (uncalibrated color pictures). (Color figure online)

envelopes of the two conditional gamuts $G_t(C_{r1})$ and $G_t(C_{r2})$ are obtained, the points of $G_t(C_{r1})$ contained into the alpha-shape enveloping $G_t(C_{r2})$ and the points of $G_t(C_{r1})$ contained into the alpha-shape enveloping $G_t(C_{r2})$ are gathered into a new set of points, from which is computed a third alpha-shape enveloping the intersection of the two conditional color gamuts. Then, the volume of this alpha-shape is computed by summing the volume of all tetrahedral contained into the alpha-shape, which can be done automatically thanks to the function *volume* in Matlab©.

Figure 6 shows another sample printed in inkjet, where two different binary color images are displayed in reflectance and 0.9-transmittance modes whose colored areas do not coincide with each other. The recto-verso print has been decomposed into four areas. In reflectance mode, areas A and B are filled with the blue color C_{r1}, and the two other areas C and D with the yellow color C_{r2}. In transmittance mode, areas A and C display the yellowish color C_{t1}, and areas B and D display the pinkish color C_{t2}. Obviously, only two halftone colors have been printed on the recto side of the paper to display the wanted colors C_{r1} and C_{r2}, whereas four different halftone colors have been printed on the verso side to display the colors C_{t1} and C_{t2}. The color matchings between areas A and C on the one hand, and between areas B and D on the other hand, were possible because both C_{t1} and C_{t2} belong to the intersection of the condition colors gamuts in transmission attached to the colors C_{r1} and C_{r2} wanted in reflection, i.e. $G_t(C_{r1}) \bigcap G_t(C_{r2})$. This latter was sufficiently large to select two colors C_{t1} and C_{t2} well distinct from each other, and therefore obtain enough contrast between the letters and the background in the image viewed in transmission mode.

Guaranteeing a good contrast in the images displayed in both reflection and transmission modes is not obvious, as illustrated by Fig. 7 through the intersection of conditional gamuts in transmission mode associated with four pairs of gray colors wanted in reflection mode (one gray color in the pair being the same in the four cases). The conditional color gamuts are represented in the same way as in Fig. 5. This figure

illustrates the fact that when colors C_{r1} and C_{r2} in the reflection mode are more distant from each other, which is preferred to have a good contrast in the image displayed in reflection mode, they generate conditional color gamuts in the transmission mode whose intersection is smaller, and it is more difficult to find in this intersection two well distinct colors C_{t1} and C_{t2}.

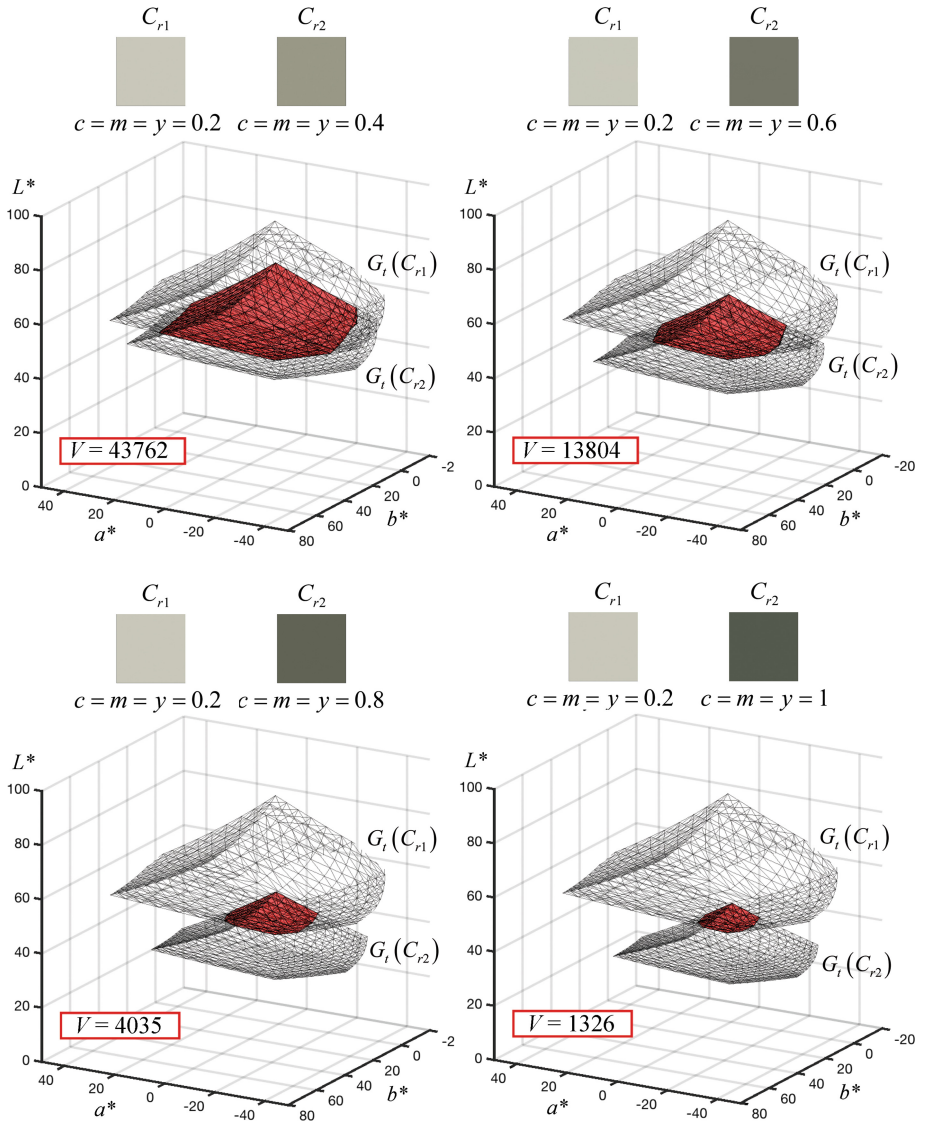

Fig. 7 Intersections of conditional color gamuts $G_t(C_{r1})$ and $G_t(C_{r2})$ in transmission mode associated with four different pairs of gray colors C_{r1} and C_{r2} wanted in reflection mode, represented in the same way as in Fig. 5. (Color figure online)

5 Contrasts in Multiple Binary Images

Let us study more deeply the influence of the color distance between the colors wanted in the reflection mode on the volume of intersection of the conditional color gamuts they generate in the transmission mode.

The volume of the intersection between two conditional color gamuts in the transmittance mode associated with two different colors selected for the reflection mode seems to be a good indicator of the possibility to find in the transmission mode two well distinct colors. We can also consider that C_{r1} has already been selected and observe how the intersection volume varies when C_{r2} is varied, as illustrated in the previous section by Fig. 7. In this case, it looks convenient to compute the ratio of the volume of $G_t(C_{r1}) \bigcap G_t(C_{r2})$ to the volume of $G_t(C_{r1})$, which defines a *relative intersection volume* induced by C_{r2} in respect to C_{r1}, denoted as $V_t(C_{r2}|C_{r1})$. The relative intersection volume tends to 1 when C_{r2} tends to C_{r1}, and it is 0 when the conditional color gamuts associated with C_{r1} and C_{r2} are disjoint. The blue curves plotted in Fig. 8 show how the relative intersection volume $V_t(C_{r2}|C_{r1})$ varies for various gray colors C_{r1} when C_{r2} is also a gray color varying from white (gray value = $c = m = y = 0$) to black (gray value 1). On the same graph is plotted in red the color distance between C_{r1} and C_{r2}, assessed by the ΔE_{94} metric. This confirms that when the two colors in the reflection mode are close from each other (small ΔE_{94} value between C_{r1} and C_{r2}) the relative intersection volume is high, and reciprocally.

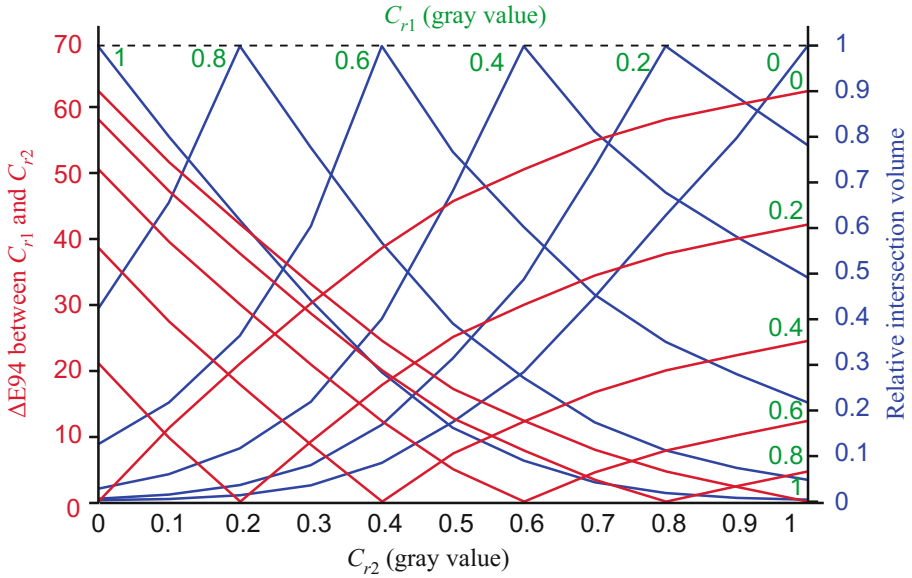

Fig. 8 Relative intersection volume $V_t(C_{r2}|C_{r1})$ of the conditional color gamuts $G_t(C_{r1})$ and $G_t(C_{r2})$ in the transmission mode associated with gray colors C_{r1} and C_{r2} wanted in reflection mode, and color distance ΔE94 between these gray colors C_{r1} and C_{r2}, plotted as functions C_{r2} from 0 (black) to 1 (white), for various gray colors C_{r1}. (Color figure online)

In order to assess more accurately the color contrast in the images, even though this concept is not clearly defined, we can consider the maximal color distance that we can find in the intersection of the conditional gamuts, in ΔE_{94} units. Alternatively to the ΔE_{94} metric, since according to Fairchild [31] humans would be more sensible to contrasts in lightness than in hue and chroma, the maximal ΔL^* value could also be considered.

The graph of Fig. 9 shows, again with gray colors, how the maximal ΔE_{94} color distance that we can obtain in the image in transmittance mode (colors C_{t1} and C_{t2}) depends on the ΔE_{94} color distance between the two colors C_{r1} and C_{r2} selected for the image in reflection mode. Once again we see that if the colors in reflectance mode are very different, the two colors in transmittance mode must be close from each other. This graph enable determining the best gray colors to select in reflection mode and transmission mode giving the best contrast in the images displayed in each one.

For example, if C_{r1} is a gray value of 0.3 (i.e. $c = m = y = 0.3$) and we want a contrast of 30 ΔE_{94} units between C_{r1} and C_{r2}, it is preferable to select a gray value for C_{r2} of 0 (no ink) or close to 1 (full coverage by the three inks), but the maximal contrast that we can obtain in transmission mode is around 35 ΔE_{94} units in the first case and only 15 ΔE_{94} units in the second case. It is therefore preferable to choose the lightest gray value for C_{r2} in reflection mode to have a better contrast in transmission mode.

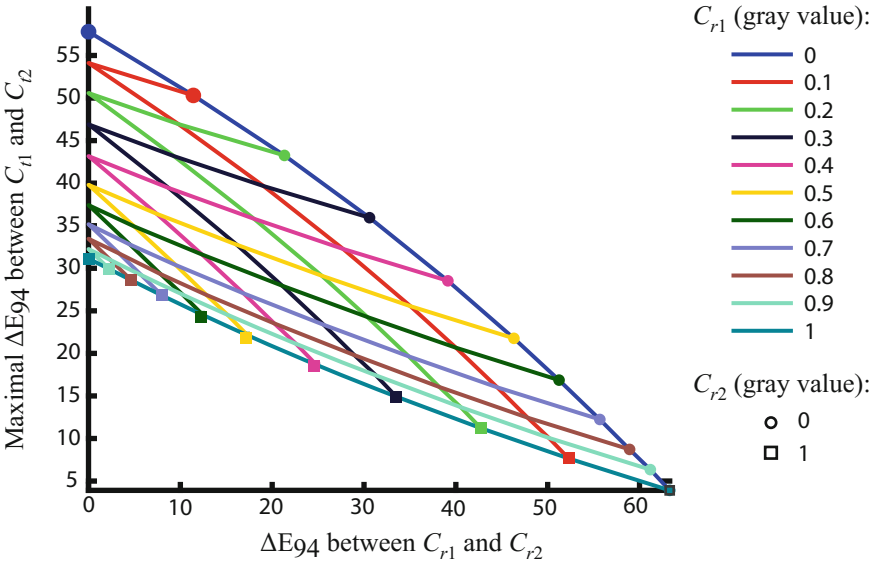

Fig. 9 Maximal ΔE_{94} value that can be obtained between the two colors in the image viewed in transmission mode, as a function of the ΔE_{94} value between the colors in the image viewed in reflection mode, for various colors C_{r1} and a variation of color C_{r2}. (Color figure online).

6 Conclusions

The present paper intended to take into account color reproduction constraints in multi-view printing for technologies able to produce supports which display different color images under different illumination or observation conditions (modes). It introduces the concept of conditional color gamut, which denotes the set of colors that can be displayed in an area of the print in one mode knowing the colors wanted for the same area in the other modes. The color matching between areas necessary to reproduce the different images in the different modes, which is not always possible, can be checked by verifying that the expected colors belong to the intersection of the conditional color gamuts of the colors wanted in the other modes. These concepts have been illustrated through the example of the recto-verso CMY printing on paper observed in two modes (reflection and transmission), which has the particularity to guarantee a good color contrast in the reflection mode in detriment to the color contrast in the transmission mode, and reciprocally. The intersection of conditional color gamuts helps to identify an optimal contrast in both modes. These concepts can be useful to help color management for multi-view printing obtained with many other technologies.

Acknowledgement. This work was supported by the French National Research Agency (ANR) within the program "Investissements d'Avenir" (ANR-11-IDEX-0007), in the framework of the LABEX MANUTECH-SISE (ANR-10-LABX-0075) of Université de Lyon.

References

1. Tzeng, D.-Y., Berns, R.S.: Spectral-based six-color separation minimizing metamerism. In: Proceedings of the IS&T/SID Color Imaging Conference, pp. 342–347 (2000)
2. Gerhardt, J., Hardeberg, J.Y.: Characterization of an eight colorant inkjet system for spectral color reproduction. In: Proceedings of the CGIV, pp. 263–267 (2004)
3. Le Moan, S., Blahová, J., Urban, P., Norberg, O.: Five dimensions for spectral color management. J. Imaging Sci. Technol. **60**(6), 60501-1–60501-9 (2016)
4. Urban, P., Berns, R.S.: Paramer mismatch-based spectral gamut mapping. IEEE Trans. Image Process. **20**, 1599–1610 (2011)
5. Baar, T., Samadzadegan, S., Ortiz-Segovia, M.V., Urban, P., Brettel, H.: Printing gloss effects in a 2.5D system. In: Proceedings of the SPIE, vol. 9018, Paper 90180 M (2014)
6. Arikan, C.A., Brunton, A., Tanksale, T.M., Urban, P.: Color-managed 3D printing with highly translucent printing materials. In: Proceedings of the SPIE, vol. 9398, Paper 93980S (2015)
7. Brunton, A., Arikan, C.A., Tanksale, T.M., Urban, P.: 3D printing spatially varying color and translucency. ACM Trans. Graph. (TOG) **37**, 157 (2018)
8. Hersch, R.D., Collaud, F., Emmel, P.: Reproducing color images with embedded metallic patterns. ACM Trans. Graph. **22**, 427–436 (2003). Proceedings of the SIGGRAPH 2003
9. Babaei, V., Hersch, R.D.: Color reproduction of metallic-ink images. J. Imaging Sci. Technol. **60,** Paper 030503 (2016)
10. Rossier, R.. Hersch, R.D.: Hiding patterns with daylight fluorescent inks. In: Proceedings of the IS&T 19th Color and Imaging Conference, pp. 223–228 (2011)
11. Pjanic, P., Hersch, R.D.: Color changing effects with anisotropic halftone prints on metal. ACM Trans. Graph. **34**, Article 167 (2015). Proceedings of the SIGGRAPH 2015

12. Destouches, N., et al.: Permanent dichroic coloring of surfaces by laser-induced formation of chain-like self-organized silver nanoparticles within crystalline titania films. In: Conference on Synthesis and Photonics of Nanoscale Materials X, Proceedngs of SPIE, vol. 8609–860905 (2013)
13. Kumar, K., et al.: Printing colour at the optical diffraction limit. Nature nanotechnology Nat. Nanotechnol. **7**, 557–561 (2012)
14. Miyata, M., et al.: Full-color subwavelength printing with gap-plasmonic optical antennas. Nano Lett. **16**(5), 3166–3172 (2016)
15. Sun, S., et al.: All-dielectric full-color printing with TiO_2 metasurfaces. ACS Nano **11**, 4445–4452 (2017)
16. Nam, H., et al.: Inkjet printing based mono-layered photonic crystal patterning for anti-counterfeiting structural colors. Sci. Rep. **6**, 30885 (2016)
17. Hébert, M., et al.: Characterization by hyperspectral imaging and hypercolor gamut estimation for structural color prints. In: Bianco, S., Schettini, R., Trémeau, A., Tominaga, S. (eds.) CCIW 2017. LNCS, vol. 10213, pp. 211–222. Springer, Cham (2017). https://doi.org/10.1007/978-3-319-56010-6_18
18. Mazauric, S., Fournel, T., Hébert, M.: Fast-calibration reflectance-transmittance model to compute multiview recto-verso prints. In: Bianco, S., Schettini, R., Trémeau, A., Tominaga, S. (eds.) CCIW 2017. LNCS, vol. 10213, pp. 223–232. Springer, Cham (2017). https://doi.org/10.1007/978-3-319-56010-6_19
19. Mazauric, S., Hebert, M., Simonot, L., Fournel, T.: Two-flux transfer matrix model for predicting the reflectance and transmittance of duplex halftone prints. J. Opt. Soc. Am. A **31**, 2775–2788 (2014)
20. Dalloz, N., Mazauric, S., Fournel, T., Hébert, M.: How to design a recto-verso print displaying different images in various everyday-life lighting conditions. In: IS&T Electronic Imaging Symposium, Materials appearance, Burlingame, USA, 30 January–2 February 2017 (2017)
21. Hébert, M., Hersch, R.D.: Reflectance and transmittance model for recto-verso halftone prints: spectral predictions with multi-ink halftones. J. Opt. Soc. Am. A **26**, 356–364 (2009)
22. Hébert, M., Hersch, R.D.: Reflectance and transmittance model for recto-verso halftone prints. J. Opt. Soc. Am. A **23**, 2415–2432 (2006)
23. Clapper, F.R., Yule, J.A.C.: The effect of multiple internal reflections on the densities of halftone prints on paper. J. Opt. Soc. Am. **43**, 600–603 (1953)
24. Williams, F.C., Clapper, F.R.: Multiple internal reflections in photographic color prints. J. Opt. Soc. Am. **43**, 595–597 (1953)
25. Hébert, M., Hersch, R.D.: Review of spectral reflectance prediction models for halftone prints: calibration, prediction and performance. Color Res. Appl. Paper 21907 (2014)
26. Hébert, M., Hersch, R.D.: Yule-Nielsen based recto-verso color halftone transmittance prediction model. Appl. Opt. **50**, 519–525 (2011)
27. Mazauric, S., Hébert, M., Fournel, T.: Revisited Yule-Nielsen model without fitting of the n parameter. J. Opt. Soc. Am. A **35**, 244–255 (2018)
28. Wyszecki, G., Stiles, W.S.: Color Science: Concepts and Methods, Quantitative Data and Formulae, 2nd edn. Wiley, Hoboken (1982)
29. Morovič, J.: Color Gamut Mapping. Wiley, Hoboken (2008)
30. Cholewo, T.J., Love, S.: Gamut boundary determination using alpha-shapes. In: Color and Imaging Conference, 7th Color and Imaging Conference Final Program and Proceedings, pp. 200–204, 5 (1999)
31. Fairchild, M.D.: Color Appearance Models, 3rd edn. Wiley, Hoboken (2013)